Dynamic interplay of Berry's phase and spectral flow in the current-voltage characteristics of a restricted class of large SNS annular Josephson junctions

Vasiliki Plerou
Department of Physics, Boston College, Chestnut Hill, Massachusetts 02167-3811

Frank Gaitan
Department of Physics, Southern Illinois University, Carbondale, Illinois 62901-4401

(Received 16 October 2000; revised manuscript received 27 November 2000; published 20 February 2001)

It has been argued that a competition arises between the Berry phase and spectral flow effects in a restricted class of large SNS annular Josephson junctions. A crossover is expected to occur in the junction response at the temperature T_* where the superconducting dynamics enters the hydrodynamic limit. For $T>T_*$, spectral flow occurs in the weak link and masks the Berry phase effects; while for $T\ll T_*$, spectral flow does not occur allowing Berry phase effects to freely influence junction dynamics. In this paper we focus on temperatures $T\lesssim T_*$ where spectral flow masking of Berry phase effects begins to switch off. In the case where a single vortex is present in the weak link, we numerically calculate the I–V curves for a restricted class of annular Josephson junctions in which nonvanishing Berry phase effects are expected to occur. We find that as Berry phase effects strengthen, distinctive shifts appear in the I–V curves which are the signature of the crossover, and provide clear targets for an experimental test of the underlying theory. We estimate T_* for a clean junction, summarize the restrictions defining the class of annular junctions in which nonvanishing Berry phase effects are expected to occur, and show how the I–V curve shifts can be understood as a consequence of: (1) a Berry phase contribution to the tunneling current density; (2) the magnetic structure of the vortex core; and (3) Bernoulli's theorem.

DOI: 10.1103/PhysRevB.63.104512 PACS number(s): 74.50.+r, 03.65.Ta, 74.60.−w

I. INTRODUCTION

Recently, there has been much progress in understanding the mechanism by which impurities and temperature can modify the nondissipative force $\mathbf{F}_{nd}$ that acts on a vortex in a type-II superconducting thin film.[1–5] It is now clear that $\mathbf{F}_{nd}$ crosses over from the (Galilean invariant) Magnus force in the collisionless limit, to the (non-Galilean invariant) Lorentz force in the hydrodynamic limit. The crossover arises from a competition between Berry phase and spectral flow effects, and the sensitivity of $\mathbf{F}_{nd}$ to impurities and temperature is a consequence of their strong influence on spectral flow. In fact, spectral flow only occurs in the hydrodynamic limit where it completely masks Berry phase effects. In the collisionless limit, however, spectral flow is absent, leaving Berry phase effects free to influence vortex motion. Kopnin and Kravtsov,[6] in much earlier work, realized that $\mathbf{F}_{nd}$ undergoes such a crossover. In effect, the more recent work has simply made more explicit the mechanism which underlies the Kopnin-Kravtsov calculation. In further work,[7] these authors demonstrated that this crossover would manifest in the Hall effect where it explained the basic trend of experiments: large (small) Hall angles θ_H in the collisionless (hydrodynamic) limit: $\theta_H\sim\pi/2$ ($\theta_H\ll 1$).

It has been argued that this competition between Berry's phase and spectral flow will also occur in a restricted class of large SNS annular Josephson junctions.[8–10] In this paper we will calculate the I–V curves for such a junction. Our goal is to obtain the experimental signature of this Berry phase/spectral flow induced crossover in the junction dynamics. Clear signatures are found, and it is hoped that they will provide motivation for an experimental test of the underlying theory. To set the stage for our Josephson junction work, we briefly summarize how the Berry phase/spectral flow mechanism works in a superconducting thin film.

In Refs. 4 and 5 it was shown that vortex motion generates a Berry phase[11] in the superconducting wave function which causes a force to act on the vortex: $\mathbf{F}_B=-(\rho_s h/2)\mathbf{v}_L\times\hat{\mathbf{z}}$. Here ρ_s is the superfluid density; h is Planck's constant; $\mathbf{v}_L$ is the vortex velocity; and $\hat{\mathbf{z}}$ is the normal to the plane of the thin film. The Berry phase force $\mathbf{F}_B$ contributes to $\mathbf{F}_{nd}$ and adds to the Lorentz force $\mathbf{F}_L=(\rho_s h/2)\mathbf{v}_T\times\hat{\mathbf{z}}$ which acts on the vortex when a transport current $\mathbf{j}_T=\rho_s e\mathbf{v}_T$ passes through the thin film. In Refs. 1–3 it was shown that spectral flow occurs inside the vortex core when the superconducting dynamics is in the hydrodynamic limit, while in the collisionless limit, spectral flow does not occur. When active, spectral flow produces a nonequilibrium occupation of the quasiparticle states bound to the vortex core which is quickly relaxed in the hydrodynamic limit. As shown by Volovik,[1] the relaxation process transfers momentum from the vortex to the lattice producing a force $\mathbf{F}_{sf}=(C_0 h/2)\mathbf{v}_L\times\hat{\mathbf{z}}$ on the vortex, with $C_0\sim\rho_s(T=0)$. $\mathbf{F}_{sf}$ only acts in the hydrodynamic limit where it contributes to $\mathbf{F}_{nd}$ along with $\mathbf{F}_B$ and $\mathbf{F}_L$. Comparison of $\mathbf{F}_{sf}$ and $\mathbf{F}_B$ shows that they: (1) have the same vector character $\mathbf{v}_L\times\hat{\mathbf{z}}$; (2) point in opposite directions; and (3) have nearly equal magnitudes. Thus, in the hydrodynamic limit, the spectral flow force effectively cancels the Berry phase force so that $\mathbf{F}_{nd}$ is entirely due to the Lorentz force. On the other hand, because there is no spectral flow in the collisionless limit, the Berry phase force is not masked

under these conditions. Thus, in the collisionless limit, $\mathbf{F}_{nd}$ is due to the Lorentz and Berry phase forces whose sum equals the Magnus force $(\rho_s h/2)(\mathbf{v}_T-\mathbf{v}_L)\times\hat{\mathbf{z}}$. Note that $\mathbf{F}_{nd}$ is distinct from dissipative and pinning forces which may also act on the vortex.

Let T_* denote the temperature at which the superconducting dynamics enters the hydrodynamic limit. In general, T_* decreases with increasing impurity concentration. We can summarize the preceding discussion of the crossover of $\mathbf{F}_{nd}$ by the formula:

$$\mathbf{F}_{nd}=\mathbf{F}_L+g(T)\mathbf{F}_B$$

$$=\frac{\rho_s h}{2}(\mathbf{v}_T-g(T)\mathbf{v}_L)\times\hat{\mathbf{z}}. \tag{1}$$

The phenomenological parameter $g(T)$ will be referred to as the (temperature-dependent) Berry phase strength, and it takes values: $0\leqslant g\leqslant 1$. In the collisionless limit ($T\ll T_*$) where spectral flow does not occur, $g=1$, and Eq. (1) reduces to the Magnus force. In the hydrodynamic limit ($T>T_*$) where spectral flow masks the Berry phase force, $g=0$, and Eq. (1) yields the Lorentz force. The crossover between these two limits begins in the temperature range $T\lesssim T_*$ where spectral flow begins to loose its ability to completely mask the Berry phase force. At these temperatures g is small ($0<g\ll 1$). This is the temperature range that will be of interest in this paper.

Returning again to Josephson junctions, it was shown in Ref. 10 that Berry's phase causes a modulation of the tunnel current density in a restricted class of large annular Josephson junctions (AJJ) in which a moving vortex is present. The necessary restrictions on the AJJ will be stated in Sec. II. The manifestation of the tunnel current density modulation is a spatially and temporally varying modification of the current drive that acts on the vortex. As pointed out in Ref. 8, spectral flow will mask this Berry phase effect in a large SNS AJJ when $T>T_*$. As mentioned above, our interest is in the temperature range $T\lesssim T_*$ at which the crossover begins to occur, going from the regime where spectral flow masks the Berry phase effects ($T>T_*$), to the regime where the Berry phase effects are active due to the absence of spectral flow ($T\ll T_*$). We will calculate the I–V curves for $T\lesssim T_*$ where the Berry phase effects strengthen as T decreases away from T_*. We will show that distinctive shifts appear in these curves as the Berry phase effects strengthen, providing clear targets for an experimental test of the underlying theory. In the following section we: (i) summarize the needed results of Ref. 10; (ii) introduce spectral flow into the junction dynamics; (iii) describe how the I–V curves are determined; and (iv) present the results of our numerical calculation. In Sec. III we show how these shifts can be understood as a consequence of the Berry phase induced modulation of the tunnel current density, the magnetic structure of the vortex core, and Bernoulli's theorem. Finally, we summarize the essential points of the paper in Sec. IV.

II. CALCULATION OF THE I–V CURVES

This section is divided into four parts. In Sec. II A we summarize how Berry's phase impacts the dynamics of a restricted class of large AJJ's (containing a single vortex) at low temperatures, and state the restrictions needed for these Berry phase effects to be observable. The reader is referred to Ref. 10 for a detailed discussion. Spectral flow effects are introduced in Sec. II B, while Sec. II C describes the calculation of the I–V curves. Finally, our numerical results are presented in Sec. II D.

A. Necessary background

For the purpose of observing Berry phase effects, not all Josephson junctions will do. As explained in detail in Ref. 10, these effects are only observable in a restricted class of large AJJs at low temperature. The precise definition of this restricted class is given below. In this paper, however, it will be sufficient to focus on a particular member of this restricted class: the planar AJJ. A careful description of a planar AJJ is given in Ref. 10. To avoid repetition, we will not repeat that description here. The annular weak link (WL) is assumed to have a bias current I passing through it. We limit ourselves to the case where a single vortex resides in the WL with magnetic flux aligned parallel to $\hat{\mathbf{z}}$. Figure 2 of Ref. 10 shows such a vortex inside the WL together with its associated screening currents. This figure also details the polar coordinate system (r,θ) used to parametrize the annular WL.

It was shown in Ref. 10 that the supercurrents flowing at the boundary of each of the junction electrodes includes a Berry phase induced contribution $\Delta\mathbf{j}_B(t)=-\rho_s e\mathbf{v}_L(t)$. Generally speaking, $\Delta\mathbf{j}_B(t)$ will have components parallel and normal to the local junction plane. The parallel component of $\Delta\mathbf{j}_B(t)$ flows *inside* the junction electrodes, and contributes to the surface supercurrents. The normal component, on the other hand, contributes to the tunneling current density and adds to the bias current density $j_T=\rho_s|e|v_T$:

$$j_{tun}(\theta,t)=j_T+\Delta\mathbf{j}_B(t)\cdot\hat{\mathbf{r}}(\theta). \tag{2}$$

The Berry phase contribution $\Delta\mathbf{j}_B(t)\cdot\hat{\mathbf{r}}(\theta)$ is intimately connected to the interesting shifts that appear in the I–V curves. These shifts are presented in Sec. II D, and their physics explained in Sec. III. The total flux of $\Delta\mathbf{j}_B$ through the WL is easily shown to vanish. Thus, the total current through the WL is solely due to the flux of the bias current density $\mathbf{j}_T$, and this flux is simply the bias current I passing through the AJJ. Thus, the Berry phase contribution to j_{tun} simply causes a redistribution of the bias current density, strengthening it in one region by reducing it in another, while still leaving the total current equal to the bias current.

As is well known,[12–14] the equation of motion for the phase dynamics of a large AJJ is a perturbed Sine-Gordon equation. The tunnel current density $j_{tun}(\theta,t)$ acts as a local energy source for the phase dynamics, producing a local driving term in the Sine-Gordon equation known as the current drive. Because $j_{tun}(\theta,t)$ contains a Berry phase contribution [see Eq. (2)], the current drive becomes sensitive to Berry's phase, and formally, this is how Berry's phase is able

to influence the junction dynamics. As shown in Ref. 10, for a clean large planar AJJ of uniform thickness at low temperature, the current drive β' is:

$$\beta' = \beta + \delta\beta(\theta,\tau). \tag{3}$$

Here $\beta = I/I_c$ is the contribution to the current drive coming from the bias current I (I_c is the junction critical current), and $\delta\beta(\theta,\tau)$ is the Berry phase induced contribution:

$$\delta\beta(\theta,\tau) = \frac{\beta}{v_T}\mathbf{v}_L(\tau)\cdot\hat{\mathbf{j}}_T(\theta). \tag{4}$$

Here $\tau = \omega_J t$ is the (dimensionless) time measured in units of the inverse Josephson plasma frequency ω_J^{-1}. The bias current density $\mathbf{j}_T(\theta)$ flows radially through the WL so that $\hat{\mathbf{j}}_T(\theta) = \pm\hat{\mathbf{r}}(\theta)$. As shown in Ref. 10, $\delta\beta(\theta,\tau)$ introduces a spatial and temporal variation into the current drive β'. We now summarize the conditions which must be satisfied if $\delta\beta(\theta,\tau)$ is to be observable.

The Berry phase induced contribution to the current drive $\delta\beta(\theta,\tau)$ was derived under the restriction that the superconducting dynamics is in the collisionless limit.[10] This corresponds to low temperature, and to AJJ's with clean superconducting electrodes and WL. It proves convenient to require that the WL have uniform thickness. This insures that the vortex will not be pinned or scattered by inhomogeneities in the WL thickness. Although it is known how to model such inhomogeneities,[13] our interest is in the competition between Berry phase and spectral flow effects. It is clearly advantageous, then, to restrict ourselves to AJJ's with WL's of uniform thickness so that pinning effects are absent, and so cannot obscure the Berry phase/spectral flow competition. Consequently, it is suggested that experiments designed to test the crossover-theory presented below use AJJ's with WL's whose thickness is as uniform as possible. Minor variation in the WL thickness is not expected to significantly alter the I–V curve shifts to be presented in Sec. II D. See Sec. IV for further discussion of this point. We now go on to show that one further restriction is necessary if $\delta\beta(\theta,\tau)$ is to be nonvanishing.

The final restriction arises from the important observation that $\delta\beta(\theta,\tau)$ is sensitive to the geometrical arrangement of the junction electrodes. This sensitivity originates in the scalar product $\mathbf{v}_L(\tau)\cdot\hat{\mathbf{j}}_T(\theta)$ which appears in Eq. (4). We see that $\delta\beta(\theta,\tau)$ will vanish for a physically uninteresting reason if the geometrical arrangement of the junction electrodes forces $\mathbf{v}_L(\tau)$ to be everywhere perpendicular to $\hat{\mathbf{j}}_T(\theta)$. This situation occurs in the original linear Josephson junction,[12] and in the well-known Lyngby AJJ (Ref. 15) (see Ref. 10). Thus, if $\delta\beta(\theta,\tau)$ is to produce observable consequences, we must restrict ourselves to AJJ's whose electrode arrangement insures that $\mathbf{v}_L(\tau)\cdot\hat{\mathbf{j}}_T(\theta)\neq 0$ for some value(s) of θ. It is this requirement on the junction electrodes that defines the restricted class of AJJ's in which the Berry phase effects are expected to be nonvanishing. Any attempt to observe the consequences of $\delta\beta(\theta,\tau)$ must be done using an AJJ belonging to this restricted class to insure that $\delta\beta(\theta,\tau)$ does not vanish for trivial reasons. As pointed out in Ref. 10, the planar AJJ and the cylindrical AJJ of Kuwada *et al.*[16] both belong to this restricted class. Having summarized the essential points concerning the Berry phase contribution to the current drive, we go on to consider spectral flow effects.

B. Spectral flow effects

As pointed out in the Introduction, in the hydrodynamic limit, spectral flow masks the Berry phase effects. This occurs for $T > T_*$. In the collisionless limit ($T \ll T_*$), however, the Berry phase effects are not masked since spectral flow does not act under these conditions. In Eq. (1) we introduced the phenomenological parameter $g(T)$ to model the crossover in $\mathbf{F}_{nd}$ due to the Berry phase/spectral flow competition. In the collisionless (hydrodynamic) limit, $g = 1(0)$, and $\mathbf{F}_{nd}$ equals the Magnus (Lorentz) force. In the crossover region $T \lesssim T_*$, $g(T)$ satisfies $0 < g \ll 1$, and g increases as T decreases away from T_*. As mentioned earlier, Makhlin and Volovik[8] have argued that a similar crossover will occur in an SNS AJJ when $T > T_*$. In the phenomenological spirit of Eq. (1), we introduce the Berry phase strength $g(T)$ into the expression for the current drive β' [see Eqs. (3) and (4)]:

$$\begin{aligned}\beta' &= \beta + g(T)\mathbf{v}_L(\tau)\cdot\hat{\mathbf{j}}_T(\theta)\\ &= \beta \pm g(T)\mathbf{v}_L(\tau)\cdot\hat{\mathbf{r}}(\theta).\end{aligned} \tag{5}$$

[Recall that $\hat{\mathbf{j}}_T(\theta) = \pm\hat{\mathbf{r}}(\theta)$ in a planar AJJ.] Replacing β' in Eq. (17) of Ref. 10 with Eq. (5) gives the following equation for the phase dynamics when $T < T_*$:

$$\frac{\partial^2\gamma}{\partial\tau^2} - \frac{\partial^2\gamma}{\partial l^2} + \sin\gamma = -a\frac{\partial\gamma}{\partial\tau} + b\frac{\partial^3\gamma}{\partial l^2\partial\tau} \pm \beta + g\mathbf{v}_L(\tau)\cdot\hat{\mathbf{r}}(l). \tag{6}$$

[Recall that $l = \theta(\overline{R}/\lambda_J)$.] It would be very interesting to use the microscopic approach of Ref. 8 to derive Eq. (6), and thus determine $g(T)$ microscopically. Here, however, we will content ourselves with a phenomenological treatment of $g(T)$. In the numerical calculation to be described below, we restrict g to values $0 \leqslant g \leqslant 0.1$ as a means of probing the crossover region $T \lesssim T_*$ where g is small.

A crude estimate of T_* was given in Ref. 10 for the case of a clean SNS AJJ. It was found that

$$T_* \sim \frac{h^2}{4\pi m k \lambda_J d}. \tag{7}$$

For typical large Josephson junctions, $\lambda_J \sim 10^{-3}$ m and $d \sim 10^{-7}$ m so that $T_* \sim 0.1$ mK. We stress that this estimate is only appropriate for a clean SNS AJJ. Generally, T_* decreases with increasing impurity concentration so that for a sufficiently dirty junction, $T_* = 0$. This underscores the importance of using a clean SNS AJJ in any experimental test of the work to be presented below. Having made this caveat about the importance of cleanliness, our estimate of T_* raises some hope that the crossover in the junction dynamics which we study below might prove observable in a sufficiently clean SNS AJJ.

C. Description of numerical calculation

Equation (6) is an example of a perturbed Sine-Gordon equation. Analytical solutions are not known for this type of equation so that a numerical approach is necessary. We adopt the Fourier-Galerkin method of Pagano *et al.*[17] We present an explicit analysis only for the lower choice of sign in Eq. (6) corresponding to $\hat{\mathbf{j}}_T(\theta) = -\hat{\mathbf{r}}(\theta)$. A similar analysis is possible for the upper choice of sign, though we shall not present it here.

The starting point is a Fourier series expansion of $\gamma(l,\tau)$ using time dependent coefficients:

$$\gamma(l,\tau) = 2\pi m\left(\frac{l}{L}\right) + \phi_0(\tau) + \sum_{n=1}^{N}\left\{\phi_n(\tau)\cos\left(\frac{2\pi n l}{L}\right) + \psi_n(\tau)\sin\left(\frac{2\pi n l}{L}\right)\right\}. \tag{8}$$

The first term on the right-hand side takes care of the periodic boundary condition,

$$\gamma(l+L,\tau) = \gamma(l,\tau) + 2\pi m. \tag{9}$$

Here L is the junction circumference in units of λ_J, and $m = 1$ for a single vortex in the junction. Inserting Eq. (8) into Eq. (6), and using the orthonormality of the trigonometric functions, we arrive at a collection of ordinary differential equations (ODE's) for the series expansion coefficients. N corresponds to the number of spatial harmonics included in the Fourier expansion. In principle, N is infinite; in practice, N is finite, and determined by the degree of accuracy one is striving for.

The presence of the Berry phase term in Eq. (6) requires three modifications of the procedure of Ref. 17. First, new terms appear in the ODE's governing the $n=1$ spatial harmonic [see Eqs. (13) below]. These terms depend on the vortex position and velocity. This gives rise to the second modification: we must locate the vortex center at each time step of the numerical integration, thus giving the vortex position, and allowing determination of the vortex velocity. The final modification is to write the scalar product appearing in Eq. (4) in a form convenient for the orthonormalization. To that end, we introduce $\overline{r} = \overline{R}/\lambda_J$ and let the vortex position at time τ be $l' = \overline{r}\theta'$. Then, $\theta' = 2\pi l'/L$, and

$$\mathbf{v}_L(\tau) = v_L(\tau)\hat{\boldsymbol{\theta}}(\theta') = v_L(\tau)[-\sin\theta', \cos\theta']. \tag{10}$$

With $\hat{\mathbf{r}}(\theta) = [\cos\theta, \sin\theta]$; and $\theta = 2\pi l/L$; we have:

$$\mathbf{v}_L(\tau)\cdot\hat{\mathbf{r}}(\theta) = v_L(\tau)\left[-\cos\left(\frac{2\pi l}{L}\right)\sin\left(\frac{2\pi l'}{L}\right) + \sin\left(\frac{2\pi l}{L}\right)\cos\left(\frac{2\pi l'}{L}\right)\right]. \tag{11}$$

For the choice of sign in Eq. (6) that we are considering, the vortex moves in the $\hat{\boldsymbol{\theta}}$ direction (see Sec. III A) so that, by Eq. (10), $v_L(\tau) > 0$. Carrying out the orthogonalization procedure, we arrive at the following set of ODE's which are to be numerically integrated:

$\underline{n=0}$

$$\ddot{\phi}_0 + a\dot{\phi}_0 + \beta = -\frac{1}{L}\int_0^L dl\,\sin\gamma, \tag{12}$$

$\underline{n=1}$

$$\ddot{\phi}_1 + \left(\frac{2\pi}{L}\right)^2\phi_1 + \left[a + b\left(\frac{2\pi}{L}\right)^2\right]\dot{\phi}_1 + gv_L\sin\left(\frac{2\pi l'}{L}\right) = -\frac{2}{L}\int_0^L dl\,\sin\gamma\cos\left(\frac{2\pi l}{L}\right); \tag{13a}$$

$$\ddot{\psi}_1 + \left(\frac{2\pi}{L}\right)^2\psi_1 + \left[a + b\left(\frac{2\pi}{L}\right)^2\right]\dot{\psi}_1 - gv_L\cos\left(\frac{2\pi l'}{L}\right) = -\frac{2}{L}\int_0^L dl\,\sin\gamma\sin\left(\frac{2\pi l}{L}\right); \tag{13b}$$

$\underline{n\geq 2}$

$$\ddot{\phi}_n + \left(\frac{2\pi n}{L}\right)^2\phi_n + \left[a + b\left(\frac{2\pi n}{L}\right)^2\right]\dot{\phi}_n = -\frac{2}{L}\int_0^L dl\,\sin\gamma\cos\left(\frac{2\pi n l}{L}\right); \tag{14a}$$

$$\ddot{\psi}_n + \left(\frac{2\pi n}{L}\right)^2\psi_n + \left[a + b\left(\frac{2\pi n}{L}\right)^2\right]\dot{\psi}_n = -\frac{2}{L}\int_0^L dl\,\sin\gamma\sin\left(\frac{2\pi n l}{L}\right). \tag{14b}$$

The terms in Eqs. (13) proportional to g result from the Berry phase contribution to the current drive $\delta\beta(\theta,\tau)$ in Eq. (6). The solutions of Eqs. (12)—(14) are used to reconstruct $\gamma(l,\tau)$. These solutions depend parametrically on a, b, L, β, and g. All our numerical integrations used $a = b = 0.02$ and $L = 4$. Three values of the Berry phase strength g were considered: $g = 0$, 0.05, and 0.10.

For given values of g and β, the DC junction voltage V is determined from the Josephson equation,

$$V = \overline{\frac{\partial\gamma}{\partial\tau}}, \tag{15}$$

where V is in units of $\hbar\omega_p/2e$, and the bar denotes a spatial and temporal average. It is important to note that, because $\gamma = \gamma(l - v_L\tau)$, V will be proportional to $-v_L$. Thus for a vortex moving in the $+\hat{\boldsymbol{\theta}}$ $(-\hat{\boldsymbol{\theta}})$ direction, the vortex velocity v_L is positive (negative), and the DC voltage V will be negative (positive). This connection between the sign of the voltage V and the sense of vortex motion will be necessary when we examine the numerical results for the I–V curves.

The I–V curve for a given Berry phase strength g is found by sweeping β from 0 up to a value β_s at which the junction

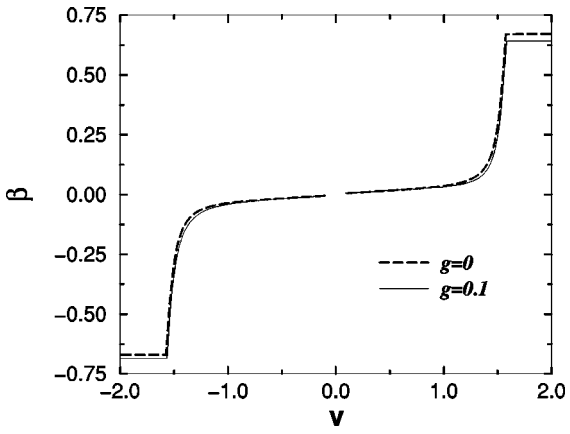

FIG. 1. Current-voltage characteristic for an SNS planar AJJ for positive and negative bias current ($g=0$ and 0.1). Positive (negative) bias β corresponds to clockwise (counter-clockwise) vortex motion around the AJJ.

switches from a stable propogating vortex state to the ''rotating'' state in which the magnetic flux is uniformly spread across the WL and the phase varies rapidly with time.[17] The signature of switching is the appearance of a horizontal plateau in the I–V curve at the critical value β_s.

D. I–V curves: Results

In Fig. 1 we plot the I–V curves for a planar AJJ for positive and negative values of the bias current β, for $g=0$ and 0.1. The current is in units of I_c and the voltage in units of $\hbar\omega_p/2e$. From the discussion at the end of Sec. II C, the portion of the curve with positive (negative) voltage corresponds to a vortex moving in the $-\hat{\boldsymbol{\theta}}$ $(+\hat{\boldsymbol{\theta}})$ direction, or equivalently, clockwise (counter-clockwise) motion around the WL. Figure 1 shows the three main features produced by Berry's phase in the I–V curves. The first is that for small bias current β, Berry's phase has little effect on the I–V curves. Next, recalling that $|V|$ is proportional to the vortex speed $|v_L|$, the second effect is that $|V|$, and hence $|v_L|$, are

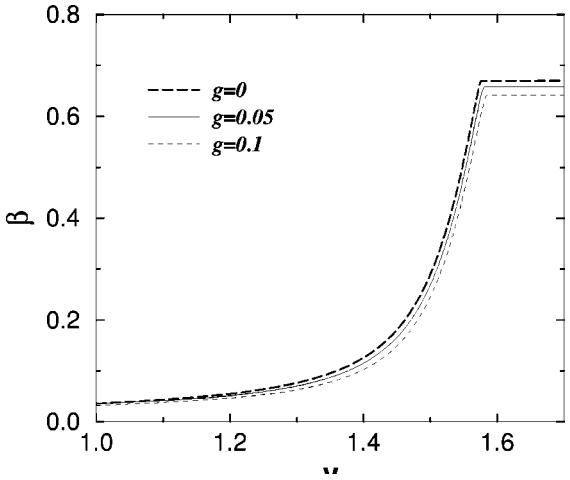

FIG. 2. Current-voltage characteristic for an SNS planar AJJ for clockwise vortex motion around the AJJ ($g=0$, 0.05, and 0.10).

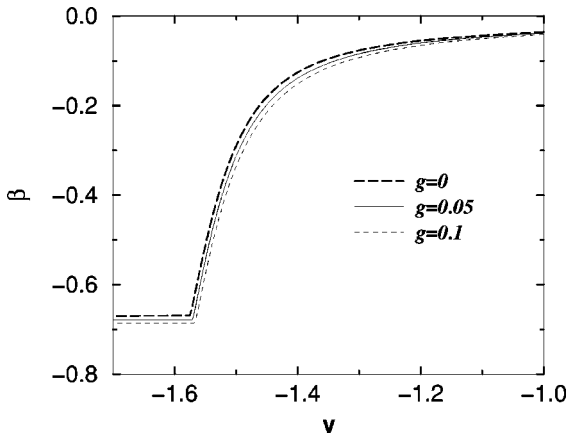

FIG. 3. Current-voltage characteristic for an SNS planar AJJ for counter-clockwise vortex motion around the AJJ ($g=0$, 0.05, and 0.10).

also sensitive to g. This manifests in the lateral shift of the vertical steps in the I–V curves with increasing g. For clockwise (counter-clockwise) vortex motion at fixed β, Fig. 1 shows that $|V|$, and hence $|v_L|$, increases (decreases) with increasing g. This behavior is more clearly seen in Figs. 2 and 3 which focus, respectively, on clockwise and counter-clockwise vortex motion. The third and final effect is that the critical current β_s at which the junction switches is sensitive to the Berry phase strength. For clockwise vortex motion, β_s is reduced as g increases; while for counter-clockwise motion, $|\beta_s|$ increases when g increases. For easy reference, we summarize these features in Table I. The variation of features 2 and 3 with the Berry phase strength g, and their smooth disappearance as $g\to 0$ $(T\to T_*^-)$ suggests that they be used as the experimental signature of the the Berry phase/spectral flow crossover.

III. PHYSICS OF I–V CURVE SHIFTS

In this section we show that the features appearing in the I–V curves when $T\lesssim T_*$ can be understood as consequences of: (1) the Berry phase contribution to the tunnel current density flowing through the WL; (2) the appearance of a negative flux region at the trailing edge of the vortex core when a large bias current passes through the WL; and (3) Bernoulli's theorem. In Sec. III A we consider temperatures $T>T_*$ where the Berry phase effects are masked by spectral flow. Here the basic arguments can be presented without the Berry phase complications. In Sec. III B we consider the case of actual interest: $T\lesssim T_*$. Here the analysis of Sec. III A is extended to include the Berry phase effects. This analysis will explain why lateral shifts appear in the I–V curves as the Berry phase effects strengthen. Finally, in Sec. III C, we explain why the critical current β_s (at which the junction switches) is sensitive to g. Before proceeding, however, two remarks are necessary:

1. As pointed out in Ref. 10, when normal currents flow parallel to the surface of the junction electrodes, dissipation occurs there, giving rise to the b term in Eq. (6). It is well known[17,18] that at large bias current this dissipation leads to

TABLE I. Summary of features produced in the I–V curves of an SNS planar AJJ by the Berry's phase for $T \lesssim T_*$.

Clockwise vortex motion	*Counter-clockwise vortex motion*
1. At small β, Berry phase effects are small.	1. At small β, Berry phase effects are small.
2. At larger, fixed β: $\lvert V\rvert\uparrow$ when $g\uparrow$.	2. At larger, fixed β: $\lvert V\rvert\downarrow$ when $g\uparrow$.
3. At switching: $\lvert\beta_s\rvert\downarrow$ when $g\uparrow$.	3. At switching: $\lvert\beta_s\rvert\uparrow$ when $g\uparrow$.

the appearance of a region of negative flux at the trailing edge of the core of a moving vortex. This region of negative flux grows with increasing bias current. Once the critical bias current β_s is reached, vortex-antivortex pairs are created at the trailing edge of the core which quickly cause the junction to switch.[17] Thus, unlike vortices in a superconducting thin film, vortices in a large Josephson junction have cores which can develop internal magnetic structure in which the flux changes sign. This has important consequences for the arguments to be presented below (see Sec. III B). We shall see that at small bias current where only positive flux is present, Berry phase effects are small. The situation is very different at large bias current where a negative flux region is also present. As we shall see, the Berry phase effects will now be significant, and are due to the interplay of: (1) the Berry phase contribution to the tunneling current density, and (2) the internal magnetic structure of the vortex core. We shall see that Bernoulli's theorem provides the basis for a qualitative analysis of the hydrodynamic force on the vortex which applies equally well to cores with or without internal magnetic structure (i.e., flux reversal). The Bernoulli analysis leads to a deeper understanding of how Berry's phase produces the I–V curve modifications presented in Sec. II D, and it nicely complements the *quantitative* analysis of Sec. II.

2. For completeness, we remind the reader of the statement of Bernoulli's theorem. For a steady, nonviscous, incompressible, and irrotational flow, the pressure P and the flow speed v maintain the sum $P+\rho v^2/2$ constant. Thus where the flow speed is large, the pressure is small, and vice versa. In the case of a wing, the flow speed is larger above the wing than below it, and so the pressure is smaller above the wing than below it. Consequently, an upward hydrodynamic force acts on the wing. Similar arguments will be used below.

A. Bernoulli analysis for $T > T_*$: Berry phase effects absent

We restrict ourselves in this subsection to temperatures $T > T_*$ where Berry phase effects are masked by spectral flow. Because of dissipation due to normal currents flowing in the surface of the junction electrodes, two cases must be considered.

Small Bias Current: For small bias current β, a region of negative magnetic flux does not appear behind the vortex.[17,18] Figure 4 shows a vortex in a large planar AJJ with magnetic flux along $\hat{\mathbf{z}}$. The screening current associated with the vortex is represented schematically by the closed loop. The bias current is assumed to pass through the junction such that $\hat{\mathbf{j}}_T(l) = -\hat{\mathbf{r}}(l)$ [recall that $l = \theta(\overline{R}/\lambda_J)$]. The bias current density $\mathbf{j}_T$ is represented by radial lines in Fig. 4.

- It is clear from Fig. 4 that $\mathbf{j}_T(l)$ enhances the flow of the screening currents at l, while reducing it at l'. Thus the pressure is less at l than at l', and a net hydrodynamic force acts on the vortex in the $+\hat{\boldsymbol{\theta}}$ direction. Thus a bias current with $\hat{\mathbf{j}}_T(l) = -\hat{\mathbf{r}}(l)$ causes a vortex to accelerate in the $+\hat{\boldsymbol{\theta}}$ direction as claimed in Sec. II C.
- Repeating this analysis for the case where $\hat{\mathbf{j}}_T(l) = +\hat{\mathbf{r}}(l)$, one finds that the vortex will be subject to a hydrodynamic force in the $-\hat{\boldsymbol{\theta}}$ direction and will accelerate in that direction.

Large Bias Current: In this case, a negative magnetic flux region does appear at the trailing edge of the vortex core. Figure 5 shows a vortex with total magnetic flux along $\hat{\mathbf{z}}$ moving in the $+\hat{\boldsymbol{\theta}}$ direction. A region of negative flux (along $-\hat{\mathbf{z}}$) has set in behind the vortex. Note, however, that the sum of the positive and negative magnetic flux remains equal to $hc/2e$. The loop with counter-clockwise circulation represents the screening current associated with the region of positive flux, while the clockwise circulating loop represents the screening current associated with the negative flux re-

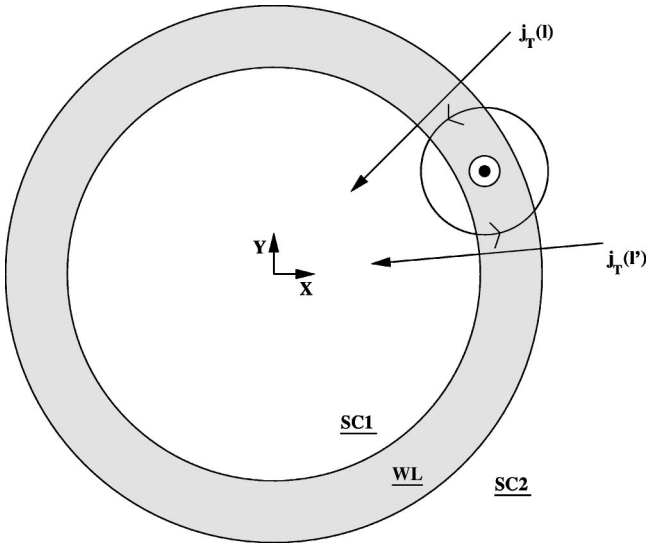

FIG. 4. A single vortex in a planar AJJ with magnetic flux along $\hat{\mathbf{z}}$ for $T > T_*$. A bias current density $\mathbf{j}_T(l)$ passes through the weak link with $\hat{\mathbf{j}}_T(l) = -\hat{\mathbf{r}}(l)$. The closed loop is a schematic representation of the screening current circulating around the vortex.

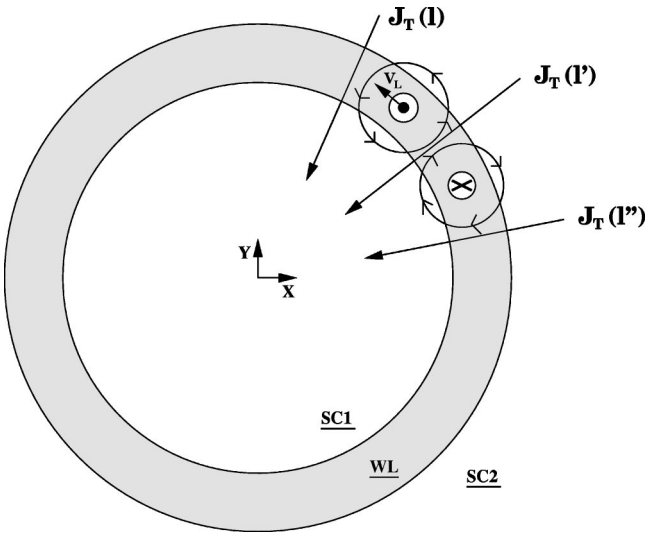

FIG. 5. A single vortex moving counter-clockwise around a planar AJJ with total magnetic flux along $\hat{\mathbf{z}}$ for $T>T_*$. The bias current β is sufficiently large to have produced a region of negative flux behind the vortex. See Sec. III A for further discussion.

gion. The radial lines represent the bias current density with direction $\hat{\mathbf{j}}_T(l)=-\hat{\mathbf{r}}(l)$, and is responsible for driving the vortex in the $+\hat{\boldsymbol{\theta}}$ direction.

• Since the flow around the positive flux region in Fig. 5 is identical with that appearing in Fig. 4, we see that the hydrodynamic force $\mathbf{F}_+$ acting on the positive flux region is in the $+\hat{\boldsymbol{\theta}}$ direction. For the negative flux region, we see that the flow associated with the screening current is reduced at l', and enhanced at l''. Thus the pressure is greater at l' than at l'', and the negative flux region is subject to a hydrodynamic force $\mathbf{F}_-$ in the $-\hat{\boldsymbol{\theta}}$ direction. The net hydrodynamic force on the vortex is $\mathbf{F}=\mathbf{F}_++\mathbf{F}_-$ (see Fig. 6). As the bias current β is increased, $\mathbf{F}_+$ and $\mathbf{F}_-$ also increase. At the critical value β_s, these forces are large enough to create vortex-antivortex pairs. At this point the traveling vortex becomes unstable: the localized magnetic flux associated with the vortex is smeared out uniformly over the WL, and the junction switches.[17]

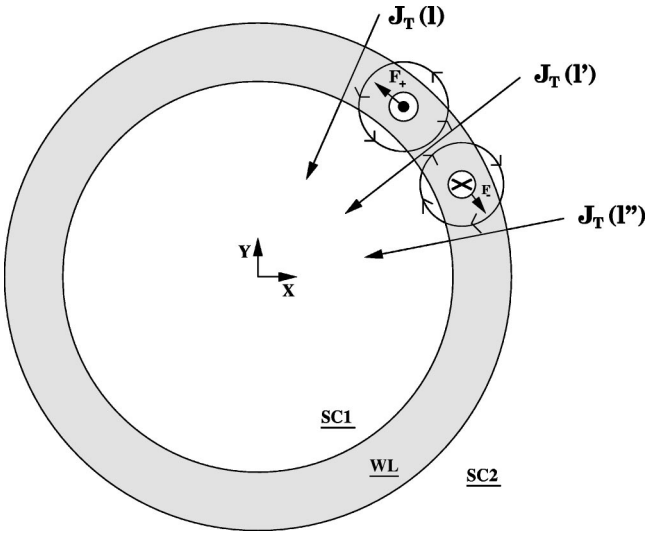

FIG. 6. The net hydrodynamic force $\mathbf{F}=\mathbf{F}_++\mathbf{F}_-$ acting on a vortex in which the bias current β has produced a region of negative flux ($T>T_*$). See Sec. III A for further discussion.

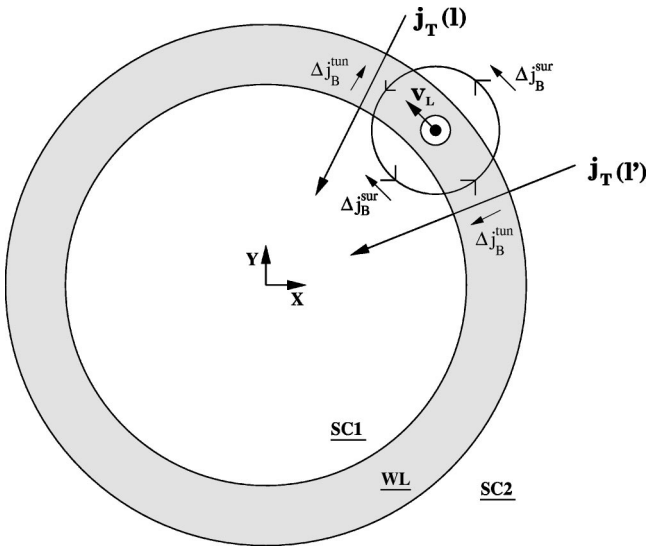

FIG. 7. A large planar AJJ containing a vortex at small bias current for $T\lesssim T_*$. The Berry phase contribution to the: (1) tunnel current density Δj_B^{tun}; and (2) junction electrode surface supercurrents Δj_B^{sur} are shown at various locations in the weak link. See Sec. III B for further discussion.

We now extend this analysis to include the Berry phase effects.

B. Bernoulli analysis for $T\lesssim T_*$: Berry phase effects present

Here we consider temperatures $T\lesssim T_*$ where the Berry phase effects first begin to appear. We again must consider the cases of small and large bias current separately. As shown in Ref. 10, and summarized in Sec. II, Berry's phase produces a contribution to the supercurrents flowing in the vicinity of the WL. The surface supercurrents flowing in the junction electrodes include the Berry phase contribution $\Delta j_B^{sur}=\Delta\mathbf{j}_B\cdot\hat{\boldsymbol{\theta}}(l)$. Depending on the sign of the scalar product, Δj_B^{sur} flows along $\pm\hat{\boldsymbol{\theta}}(l)$. The tunneling current density includes a Berry phase contribution $\Delta j_B^{tun}=\Delta\mathbf{j}_B\cdot\hat{\mathbf{r}}(l)$, and depending on the sign of the scalar product, it flows along $\pm\hat{\mathbf{r}}(l)$. It is very important to note that only Δj_b^{tun} actually flows in the WL; Δj_B^{sur} flows inside, and at the surface of, the junction electrodes. Using Eqs. (5), (4), and (2), one can show that $\Delta\mathbf{j}_B(g)=gJ_c\mathbf{v}_L$, where g is the Berry phase strength. Thus, both components of $\Delta\mathbf{j}_B$ vanish when $T=T_*$ $(g=0)$, and grow larger as T decreases away from T_* (i.e., as g increases). In this subsection we repeat the Bernoulli analysis of Sec. III A, this time including Δj_B^{sur} and Δj_B^{tun} in the analysis. We again consider a vortex with total magnetic flux along $\hat{\mathbf{z}}$.

Small Bias Current: Figure 7 shows a large planar AJJ

with a bias current density for which $\hat{\mathbf{j}}_T(l) = -\hat{\mathbf{r}}(l)$. This causes the vortex to move in the $+\hat{\boldsymbol{\theta}}$ direction as discussed in Sec. III A. Thus $\mathbf{v}_L = v_L \hat{\boldsymbol{\theta}}$, and $v_L > 0$. Note that since $\Delta \mathbf{j}_B = g J_c \mathbf{v}_L$, its direction is parallel to $\mathbf{v}_L$. In Fig. 7 we draw Δj_B^{sur} and Δj_B^{tun} at various locations on the WL. As mentioned above, their directions are found by evaluating the scalar product of $\Delta \mathbf{j}_B$ with $\hat{\boldsymbol{\theta}}(l)$ and $\hat{\mathbf{r}}(l)$, respectively.

• Our first observation is that Berry's phase produces a *hydrodynamic* force which has an $\hat{\mathbf{r}}$ component (though see the related Meissner effect remark below). Figure 7 shows that Δj_B^{sur} reduces the screening flow present in the surface of SC1, while enhancing the screening flow in the surface of SC2. Thus a hydrodynamic force acts in the $+\hat{\mathbf{r}}(l)$ direction. This corresponds to the Berry phase force contribution in Eq. (1) which can be written as $\Delta \mathbf{j}_B \times \boldsymbol{\Gamma}$, where $\boldsymbol{\Gamma} = (hc/2e)\hat{\mathbf{z}}$ is the magnetic flux associated with the vortex. This clearly acts in the $\hat{\mathbf{r}}(l)$ direction. It is very important to note, however, that due to the Meissner effect, the SC electrodes always apply a counter-force on the vortex in the radial direction which insures that the *net radial force* on the vortex exactly equals the centripetal force needed to keep it moving within the annular WL. Thus this radial Berry phase effect is always neutralized by the Meissner effect.

• Berry's phase also produces a contribution to the $\hat{\boldsymbol{\theta}}$ component of the hydrodynamic force. The magnitude of this force depends on the size of the bias current β. We now show that at small bias current, this force is at best a small perturbation, while at large bias current, it makes an important contribution to the driving force on a vortex. Note that the existence of this force is not predicted by Eq. (1) which applies to a vortex with a core inside which the magnetic flux does not change sign.[5,10] We remind the reader that these conditions do *not* occur in a large AJJ at large bias current when normal current dissipation occurs at the surface of the junction electrodes. One needs to recognize then that, *under these conditions*, Eq. (1) becomes unreliable because its derivation does not account for the effects of the negative flux region on $\mathbf{F}_{nd}$. Consequently, it is no longer the final word on the driving force on a vortex in such an AJJ. The final word, quantitatively, is Eq. (6). For a qualitative analysis, Bernoulli's theorem provides a better starting point than Eq. (1) since it applies equally well to cores in which the magnetic flux may or may not change sign. In the present case of small bias current, we see from Fig 7 that Δj_B^{tun} acts to reduce the screening flow ahead of, and also behind, the vortex relative to the corresponding situation shown in Fig. 4 where $T > T_*$ and the Berry phase effects are absent. This causes the pressure to rise both ahead of, and behind, the vortex relative to the situation in Fig. 4. Consequently, the pressure differential on the vortex at *small bias current* β is, at most, only slightly modified by Berry's phase. Thus, the Berry phase contribution to the $\hat{\boldsymbol{\theta}}$ component of the hydrodynamic force is expected to be (at best) small for small bias current, and one expects Berry's phase to have minor effect on the I–V curves at small β. This is in agreement with what was found numerically, and explains the first entry in Table I. This also agrees with Eq. (1) which predicts that Berry's phase will only contribute to the $\hat{\mathbf{r}}$ component of the hydrodynamic force on the vortex. (As discussed above, this force is neutralized by the Meissner effect.) Note that this agreement with Eq. (1) at small bias current is quite necessary since only positive flux is present inside the core under this condition, and so Eq. (1) properly accounts for the Berry phase effects. We now show, however, that at *large* bias current β where a region of negative magnetic flux sets in behind the vortex, the Berry phase contribution to the $\hat{\boldsymbol{\theta}}$ component of the hydrodynamic force is *not* small.

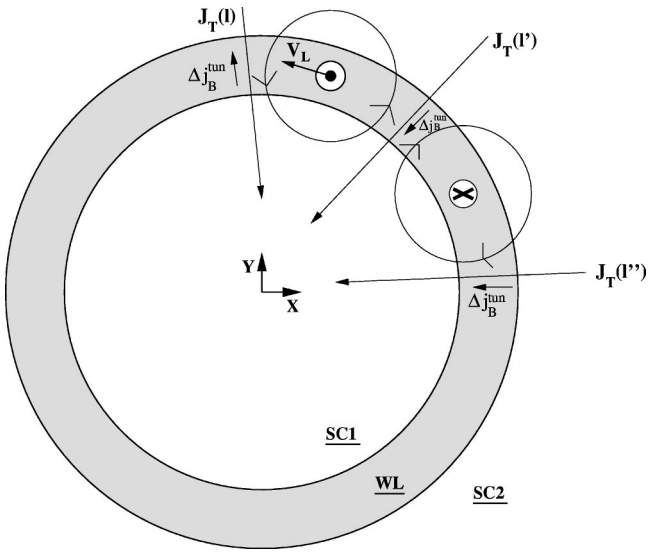

FIG. 8. A large planar AJJ containing a vortex at a large bias current for $T \lesssim T_*$. A region of negative flux has been produced behind the vortex by the bias current. The Berry phase contribution to the tunnel current density Δj_B^{tun} is shown at various locations in the weak link. See Sec. III B for further discussion.

Large Bias Current: Figure 8 shows a vortex moving in the $+\hat{\boldsymbol{\theta}}$ direction with magnetic flux along $\hat{\mathbf{z}}$. The bias current density has $\hat{\mathbf{j}}_T(l) = -\hat{\mathbf{r}}(l)$. Δj_B^{tun} is drawn at various locations along the WL. As mentioned above, its direction is determined by the sign of the scalar product of $\Delta \mathbf{j}_B$ with $\hat{\mathbf{r}}(\theta)$. Note that although the magnitude of Δj_B^{tun} varies with θ, we ignore this variation when drawing Fig. 8. We do not include Δj_B^{sur} in the figure as its effect is always masked by the Meissner effect as discussed above. The bias current β is assumed to be large enough to produce a region of negative flux behind the vortex.

• Because the superflow around the positive flux region in Fig. 8 is identical with the superflow in Fig. 7, we know that Δj_B^{tun} will only contribute slightly to the hydrodynamic force $\mathbf{F}'_+$ acting on the positive flux region in Fig. 8. If we denote by $\mathbf{F}_+$ the corresponding force on the positive flux region when Berry phase effects are absent (see Fig. 6), we see that $F'_+ \approx F_+$. We now consider the region of negative flux, and will similarly denote the hydrodynamic force on this region by $\mathbf{F}'_-$ ($\mathbf{F}_-$) in the case where Berry phase effects are (are not) present. From Fig. 8 we see that at l', Δj_B^{tun}

causes the screening flow to be reduced even more than it was in Fig. 5 where the Berry phase effects were absent. Thus the pressure at l' is larger when the Berry phase effects are present than when they are absent. Similarly, Figs. 8 and 5 show that, at l'', the flow associated with the screening currents is enhanced by Δj_B^{tun} beyond the enhancement already occuring in Fig. 5 where the Berry phase effects are absent. Thus the pressure at l'' is smaller when Berry phase effects are present than when they are absent. Consequently, the pressure differential on the negative flux region is in the $-\hat{\boldsymbol{\theta}}$ direction, and will be *larger* when the Berry phase effects are present than when they are absent: $F'_- > F_-$. Thus the interplay of the Berry phase effects with the negative flux region produces a force in the $-\hat{\boldsymbol{\theta}}$ direction. For a vortex moving counter-clockwise around the WL, this is a retarding force which grows as g increases. Thus the total driving force $\mathbf{F}' = \mathbf{F}'_+ + \mathbf{F}'_-$ acting on a vortex moving in the $+\hat{\boldsymbol{\theta}}$ direction (counter-clockwise motion around the WL) decreases as the Berry phase effects strengthen. Because the total driving force decreases as the Berry phase effects strengthen (g increases), it follows that, in steady state, the vortex speed $|v_L|$ will decrease as g increases. We now show that the sensitivity of $|v_L|$ to g is inherited by the DC voltage V.

- As pointed out in Sec. II C, since the absolute value of the voltage $|V|$ is proportional to the vortex speed $|v_L|$, slower speed corresponds to smaller voltage $|V|$. For the I–V curves, this means that, for a given $|\beta|$, a vortex moving counter-clockwise around the WL should have $|V|$ decrease with increasing g. This is exactly what is found numerically (see Figs. 1 and 3), and summarized in entry 2 of the right-hand column of Table I.
- Repeating the above analysis for a vortex moving clockwise ($-\hat{\boldsymbol{\theta}}$ direction) around the WL, one finds that $F'_+ \approx F_+$, and $F'_- < F_-$. Thus the net driving force $\mathbf{F}' = \mathbf{F}'_+ + \mathbf{F}'_-$ *increases* with increasing g since the retarding component F'_- *decreases* with increasing g. Thus, in this case, at given $|\beta|$, the steady state vortex speed $|v_L|$ should increase with increasing g, causing the voltage $|V|$ to increase with increasing g. This is what is found numerically (see Figs. 1 and 2), and summarized in entry 2 in the left-hand column of Table I.

We see that we can understand the lateral shift of the I–V curves encountered in our numerical results as a manifestation of: (1) the Berry phase contribution to the tunnel current density Δj_B^{tun}; (2) the internal magnetic structure of the vortex core; and (3) Bernoulli's theorem.

C. Consequences of the Berry's phase for junction switching

Tables II and III list the numerical values found for β_s and V_s at which switching occurred for different values of g, and correspond to clockwise and counter-clockwise vortex motion, respectively. Also listed is the DC power, $P_s = \beta_s V_s$; and the percent change in $P_s(g)$: $\delta P_s = 100|P_s(g) - P_s(0)|/P_s(0)$. We see that in all cases, $P_s(g)$ varies by no more than 3.5%, and thus is a slowly varying function of g over the range of values considered. Ignoring this slight variation then, $P_s(g_1) = P_s(g_2)$, so that

$$\left|\frac{\beta_s(g_2)}{\beta_s(g_1)}\right| = \left|\frac{V_s(g_1)}{V_s(g_2)}\right|. \tag{16}$$

Let $g_2 > g_1$. For clockwise vortex motion, Table II shows that $V_s(g_1)/V_s(g_2) < 1$. This is a consequence of the Berry phase effects, as discussed in Sec. III B. From Eq. (16) we see that $\beta_s(g_2) < \beta_s(g_1)$, so that the switching plateau in the first quadrant of Fig. 1 should move downward with increasing g. This is exactly what is found in our numerical results (see Figs. 1 and 2).

A similar analysis for counter-clockwise vortex motion indicates that, for $g_2 > g_1$, $|\beta_s(g_2)| > |\beta_s(g_1)|$. Thus the switching plateau in the third quadrant of Fig. 1 should move downward with increasing g, exactly as observed in Figs. 1 and 3.

We see that entry 3 of Table I can be understood as a consequence of: (1) the Berry phase induced lateral shift of the I–V curves discussed in Sec. III B: and (2) the slow variation of $P_s(g)$ with g when $T \lesssim T_*$.

TABLE II. Switching values for clockwise vortex motion as a function of g.

g	$\beta_s(g)$	$V_s(g)$	$P_s(g)$	δP_s
0.00	0.668365	1.57525	1.0529	0.00%
0.05	0.656570	1.57957	1.0371	1.50%
0.10	0.641204	1.58406	1.0157	3.53%

IV. SUMMARY OF ESSENTIAL POINTS

In this paper we have studied the Berry phase/spectral flow induced crossover in the dynamics of a restricted class of large SNS AJJ's. The crossover is expected to occur at the temperature T_* at which the superconducting dynamics enters the hydrodynamic limit. In this limit ($T > T_*$), spectral flow is active and causes a masking of the Berry phase effects. In the collisionless limit ($T \ll T_*$), spectral flow does not act, leaving the Berry phase effects free to influence junction dynamics. We have focused on temperatures $T \lesssim T_*$ where the Berry phase effects start to become observable, and strengthen as T decreases away from T_*.

We numerically evaluated the I–V curves for this restricted class of large SNS AJJ's in the case where a single vortex is present in the WL, and found that a number of interesting shifts appear in the I–V curves as the Berry phase effects strengthen. These shifts provide clear targets for an

TABLE III. Switching values for counter-clockwise vortex motion as a function of g.

g	$\beta_s(g)$	$V_s(g)$	$P_s(g)$	δP_s
0.00	−0.668365	−1.57525	1.0529	0.00%
0.05	−0.678350	−1.57122	1.0659	1.23%
0.10	−0.684945	−1.56695	1.0732	1.93%

experimental test of the crossover theory (see Figs. 1–3 and Table I).

We discussed a number of conditions which crucially effect the observability of the crossover (see Sec. II B):

1. The geometry of the junction electrodes must be such that the vortex velocity $\mathbf{v}_L(t)$ and the local tunnel current density $\mathbf{j}_T(\theta)$ satisfy $\mathbf{v}_L(t)\cdot\mathbf{j}_T(\theta)\neq 0$ for some value(s) of θ. This condition defines the restricted class of AJJ's in which the Berry phase effects are expected to occur. As shown in Ref. 10, it is *not* satisfied in the traditional linear Josephson junction, nor in the well-known Lyngby AJJ. Thus these junctions should not be used in a search for the Berry phase/spectral flow induced crossover. Ref. 10 also showed that a planar AJJ and the cylindrical AJJ of Kuwada *et al.*[16] both belong to this restricted class, and thus are suitable for use in such a search.

2. Because the crossover temperature T_* decreases as the impurity concentration increases, for sufficiently dirty junctions, it can vanish: $T_*=0$. Clearly then, an experimental search for the crossover must use a clean large SNS AJJ so as to maximize T_*. A crude estimate for such an AJJ found that $T_*\sim 0.1mK$. Although the estimate is crude, it gives some hope that the crossover might prove observable in a sufficiently clean large SNS AJJ belonging to the restricted class defined in 1.

3. We also require the WL thickness to be as uniform as possible. This reduces the possibility of pinning or scattering of the vortex by inhomogeneities in the junction thickness which might otherwise act to obscure the Berry phase/spectral flow competition. Minor variations in the WL thickness are expected to predominantly influence the junction dynamics at small bias current. Large bias currents are sufficiently energetic to de-pin the vortex and overwhelm the scattering effects produced by such minor variations in WL thickness. Since the I–V curve shifts occur at large bias current, this requirement should be sufficient to protect them from the effects of minor thickness inhomogeneities.

We have also discussed at great length (Sec. III) the physics underlying the Berry phase induced shifts in the I–V curves. We have shown that they arise from an interesting interplay of: (1) the Berry phase contribution to the local tunnel current density; (2) the internal magnetic structure of the vortex core arising, at large bias current, from dissipation produced by normal currents flowing at the surface of the junction electrodes; and (3) Bernoulli's theorem. This interplay was shown to produce a hydrodynamic force in the $\hat{\boldsymbol{\theta}}$ direction whose magnitude is a function of the Berry phase strength g, and whose contribution to the driving force on a vortex is the source of the interesting new shifts in the I–V curves. Such a force is *not* expected on the basis of Eq. (1). It is important to note, however, that the derivation of Eq. (1) assumed a vortex core in which the magnetic flux does not change sign.[5,10] This condition does *not* prevail in a large AJJ at large bias current with normal current dissipation occuring at the surface of the junction electrodes. In fact, as seen in Sec. III B, the appearance of a region of reversed magnetic flux at the trailing edge of the vortex core under these conditions is crucial for producing a Berry phase force in the $\hat{\boldsymbol{\theta}}$ direction. One needs to recognize, then, that Eq. (1) becomes unreliable when a region of reversed magnetic flux is present inside the vortex core because its derivation does not account for the effects of the reversed flux on $\mathbf{F}_{nd}$. In such cases, Bernoulli's theorem provides a better starting point for a qualitative analysis since it easily takes into account the presence of a negative flux region in the core.

Further work is possible in a number of directions. For the case of a single vortex in the WL, it would be useful to examine the effects produced on the Berry phase induced shifts in the I–V curves by variation of the dissipation strengths a and b which appear in Eq. (6). It would also be interesting to derive an expression for g from the microscopic theory of Ref. 8. We have also examined the cases where two and three vortices are present in the WL, and have found interesting preliminary results associated with the vortex bunching transition. This looks to be a promising area for further research. We hope to report on these results in the future.

We strongly hope that this work, together with Ref. 10, might encourage an experimental search for the Berry phase/spectral flow induced crossover which has been the subject of this paper.

ACKNOWLEDGMENT

We would like to thank T. Howell III for continued support.

[1] G.E. Volovik, Zh. Éksp. Teor. Fiz. **104**, 3070 (1993) [JETP **77**, 435 (1993)].
[2] M. Stone, Phys. Rev. B **54**, 13 222 (1996).
[3] N.B. Kopnin, G.E. Volovik, and Ü. Parts, Europhys. Lett. **32**, 651 (1995).
[4] P. Ao and D.J. Thouless, Phys. Rev. Lett. **70**, 2158 (1993).
[5] F. Gaitan, Phys. Rev. B **51**, 9061 (1995).
[6] N.B. Kopnin and V.E. Kravtsov, Zh. Éksp. Teor. Fiz. **71**, 1644 (1976) [Sov. Phys. JETP **44**, 861 (1976)].
[7] N.B. Kopnin and V.E. Kravtsov, Pis'ma Zh. Éksp. Teor. Fiz. **23**, 631 (1976) [JETP Lett. **23**, 578 (1976)].
[8] Y.G. Makhlin and G.E. Volovik, Pis'ma Zh. Éksp. Teor. Fiz. **62**, 923 (1995) [JETP Lett. **62**, 941 (1995)].
[9] F. Gaitan and S.R. Shenoy, Phys. Rev. Lett. **76**, 4404 (1996).
[10] F. Gaitan, preceding paper, Phys. Rev. B **63**, 104511 (2001).
[11] M.V. Berry, Proc. R. Soc. London, Ser. A **392**, 45 (1984).
[12] B.D. Josephson, Adv. Phys. **14**, 419 (1965).
[13] D.W. McLaughlin and A.C. Scott, Phys. Rev. A **18**, 1652 (1978).
[14] A.C. Scott, *Active and Non-Linear Wave Propogation in Electronics* (Wiley-Interscience, New York, 1970).
[15] A.V. Ustinov, T. Doderer, R.P. Huebener, N.F. Pedersen, B. Mayer, and V.A. Oboznov, Phys. Rev. Lett. **69**, 1815 (1992).
[16] M. Kuwada, Y. Onodera, and Y. Sawada, Phys. Rev. B **27**, 5486 (1983).
[17] S. Pagano, M.P. Soerensen, P.L. Christiansen, and R.D. Parmentier, Phys. Rev. B **38**, 4677 (1988).
[18] A. Davidson, N.F. Pedersen, and S. Pagano, Appl. Phys. Lett. **48**, 1306 (1986).